An improved solution of the gravity field of Mars (GMM-2B) from Mars Global Surveyor

F. G. Lemoine, D. E. Smith, and D. D. Rowlands

Laboratory for Terrestrial Physics, NASA Goddard Space Flight Center, Greenbelt, Maryland, USA

M. T. Zuber[1] and G. A. Neumann [1]

Department of Earth, Atmospheric, and Planetary Sciences, Massachusetts Institute of Technology
Cambridge, Massachusetts, USA

D. S. Chinn[1] and D. E. Pavlis[1]

Raytheon ITSS Corp., Lanham, Maryland, USA

Abstract. A spherical harmonic solution of the Mars gravity field to degree and order 80, Goddard Mars Model 2B (GMM-2B), has been developed using X band tracking data of Mars Global Surveyor (MGS) from October 1997 to February 2000 and altimeter crossovers formed from the Mars Orbiter Laser Altimeter (MOLA) data between March and December 1999. During the mapping mission, MGS was located in a near-polar (92.9° inclination) and near-circular orbit at a mean altitude of 400 km. The tracking data from this orbit provide a detailed, global, and high resolution view of the gravity field of Mars. Mars gravity solutions are stable to 60×60 even without application of a Kaula power law constraint. The Valles Marineris is resolved distinctly with lows reaching -450 mGals. Olympus Mons and its aureole are both separately resolved, and the volcano has a peak anomaly of 2950 mGals. The global correlation of the GMM-2B gravity coefficients with MOLA-derived topography is 0.78 through degree 60, and the correlation remains above 0.6 through degree 62. The global gravity anomaly error predicted from the GMM-2B error covariance through 60×60 is 11 mGal. The global geoid error from GMM-2B through 60×60 is 1.8 m. MGS orbit quality using GMM-2B, as measured by overlapping orbital arcs, is 1 m in the radial direction and 10 m in total position.

1. Introduction

Prior to the arrival of the Mariner 9 and Viking Orbiter missions at Mars, knowledge of the Mars gravity field was limited to estimates of the Mars gravitational constant (*GM*, or the universal constant of gravitation multiplied by the planet mass) and the planet's oblateness. Estimates were obtained from studies of the motions of the natural satellites of Mars [e.g., *Wilkins,* 1967; *Sinclair,* 1972] or from flybys of Mars by Mariner 4 and Mariner 6 [*Null,* 1969; *Anderson et al.,* 1970]. Estimates of the Mars *GM* were also obtained from indirect measurement of how Mars perturbs the orbits of the other planets. For example, *Ash et al.* [1967] combined optical and radar observations of the inner planets to estimate planetary ephemerides and astronomical constants, including the Mars *GM*.

The first insights into the unique character of the Mars gravity field came from the analysis of the Mariner 9 tracking data. The Mariner 9 spacecraft mapped Mars for 11 months starting in November 1971, from an eccentric, near 12 hour orbit, with periapsis altitudes of 1390-1650 km at 64° inclination. *Lorell et al.* [1973], *Born* [1974], *Reasenberg et al.* [1975], and *Sjogren et al.* [1975] found that the Mars gravity field was much rougher than that of the Earth with total geoid variations of up to 2000 m (compared to no more than 200 m for the Earth). A geoid high of over 1200 m was detected in Tharsis and revealed the strong C22/S22 character of the Mars gravity field.

Viking Orbiter 1 was inserted into Mars orbit in July 1976, and Viking Orbiter 2 followed in August 1976. As detailed by *Snyder* [1977, 1979], and *Lemoine* [1992], the spacecraft occupied eccentric orbits at a variety of periapsis altitudes and inclinations. *Gapcynski et al.* [1977] used a limited amount of Mariner 9 and Viking Orbiter data to determine a degree and order 6 spherical harmonic solution. *Christensen and Williams* [1979] and *Christensen and Balmino* [1979] combined more extensive sets of Mariner 9 and Viking data to determine spherical harmonic solutions to degree and order 12.

---

[1]Also at Laboratory for Terrestrial Physics, NASA Goddard Space Flight Center, Greenbelt, Maryland, USA.

The periapsis altitudes of Viking Orbiters 1 and 2 were lowered to 300 km in March 1977 and October 1977, respectively. At this altitude the tracking data have sensitivity to short-wavelength features of the Mars gravity field. *Sjogren et al.* [1978] and *Sjogren* [1979] used the low-altitude data to map the Mars gravity field from 30°S to 65°N. They identified the large anomaly associated with Olympus Mons (344 mGals at 275 km altitude), a mascon in the Isidis basin, and the correlation of anomalies with other volcanic features such as Elysium, Alba Patera, and Arsia Mons. *Balmino et al.* [1982] combined nearly all available Mariner 9 and Viking Orbiter tracking data to determine a degree and order 18 spherical harmonic solution. The size of the field was chosen in view of the distribution of the available data below 700 km altitude.

In preparation for the Mars Observer mission, *Smith et al.* [1993] reprocessed the Viking Orbiter and Mariner 9 tracking data. Their objective was to take advantage of the advances in computer capabilities and develop a solution to sufficiently high degree that would exhaust the signal in the data. A degree and order 50 solution (Goddard Mars Model-1, or GMM-1) was obtained using a Kaula power law constraint to stabilize the solution at the higher degrees due to uneven data distribution. *Konopliv and Sjogren* [1995] developed Mars50c, a 50th degree and order model from solely Mariner 9 and Viking Orbiter tracking using a spatial a priori constraint method. In the development of this model the Kaula power law constraint was effectively relaxed over the Tharsis volcanos, allowing greater power in the gravity field over this area. For example, in GMM-1 the anomaly over Olympus Mons (266°E, 18°N) was 1159 mGal (evaluated to 50 × 50), compared to 2060 mGal with Mars50c (evaluated to 50 × 50) and 2950 mGal (evaluated to 60 × 60) with the Mars Global Surveyor (MGS) derived model discussed in this paper, GMM-2B. In the absence of adequate data, the Kaula power law constraint effectively biases the coefficients toward zero. In addition, the data were weighted more heavily in Mars50c than in GMM-1.

The tracking data obtained from MGS differ in two fundamental respects from the earlier tracking data obtained by Mariner 9 and the Viking Orbiters. Most important, in the mapping phase of its mission, MGS is located in a low-altitude, near-circular (400 km mean altitude), and polar (92.9° inclination) orbit. This compares to the highly eccentric, near 12 hour and near 24 hour orbits of Mariner 9 and the Viking Orbiters. Thus, MGS obtains global coverage at low altitude, compared to the partial low-altitude coverage obtained by Viking Orbiters 1 and 2. Second, MGS carries an X band transponder rather than the S band transponders carried by the previous generation of Mars Orbiters [*Tyler et al.*, 1992; *Tyler et al.*, this issue]. The X band frequency of ~8 GHz used on MGS is less sensitive to noise and disturbances from the Earth ionosphere and solar plasma than the S band frequency of ~2.1 GHz used on the tracking systems of the earlier missions. MGS achieves a data noise of 0.1 mm/s over a 10 s counting interval. The best performance achieved in orbital arcs that used the Viking S band Doppler data was 2.5 mm/s over a count interval of 60 s [*Lemoine,*

1992]. Improvements in data quality can also be ascribed to the upgrades in equipment at the tracking sites of the Deep Space Network (for instance, installation of better frequency standards). In addition, with MGS the timing and duration of attitude control system maneuvers are documented systematically, whereas for the Viking Orbiters and Mariner 9, this information is not always readily available, especially many years after the end of those spacecraft missions.

In this paper we present the results of our latest analysis of the MGS tracking data and the derivation of an 80 × 80 spherical harmonic model of the Mars gravity field. In comparison, the results presented by *Smith et al.* [1999b] were based only on data obtained in the Gravity Calibration Orbit (February 1999) and in Fixed High Gain Antenna Mapping (March 1999). Compared to the field discussed by *Zuber et al.* [2000], we have reiterated all the least squares normal equations, added more than 5 months of tracking in mapping and introduced additional altimeter crossovers into the solution.

2. Data

2.1. Mission Summary

We first review the different mission phases of Mars Global Surveyor after its arrival at Mars in order to understand when usable tracking data were obtained for gravity model determination. MGS entered Mars orbit on September 12, 1997. The initial plans called for 4 months of aerobraking followed by entry into the mapping orbit by early 1998. However, concerns with the -*Y* solar panel led to the suspension of the first phase of aerobraking in October 1997 and to the development of an alternate plan to reach the mapping orbit. During this 3 week suspension of aerobraking (known as Hiatus), some science data including Mars Orbiter Laser Altimeter (MOLA) data, were obtained. Further aerobraking took place in two phases: November 1997 to March 1998 and September 1998 to February 1999 [*Esposito et al.,* 1998; *Johnston et al.,* 1999]. From March 1998 through September 1998, MGS was located in an elliptic, 11.6 hour phasing orbit with a periapsis height of 170 km. Interim science data, including altimeter data and tracking data were collected during this period known as the Science Phasing Orbit (SPO). Periapsis during SPO was located in the northern hemisphere above 60°N (see Table 1).

Aerobraking ended on February 4, 1999, when MGS attained its designated low-altitude orbit. For several weeks after the termination of aerobraking, MGS was in the gravity calibration phase of its mission. The spacecraft was maintained in a quiescent state, with the high-gain antenna pointed continuously at the Earth in order to acquire the best possible tracking data. MGS was placed in a frozen orbit on February 19, 1999, in order to minimize orbit-to-orbit altitude variations [*Cutting et al.,* 1978]. In the MGS mapping orbit, periapsis does not precess around the planet, but rather librates in a small band about the South Pole.

The first altimeter data in the mapping phase were returned on February 28, 1999, and formal mapping operations commenced on March 8, 1999. Throughout March

Table 1. MGS Orbit Characteristics

Mission Phase[a]	Dates		Orbital Period, hours	Periapse Height, km	Periapsis Latitude[b]
	From	To			
Insertion	Sept. 12, 1997	Sept. 16, 1997	44.99	263	31°N
Hiatus	Oct. 13, 1997	Nov. 7, 1997	35.43	170	35°N
SPO-1	March 27, 1998	May 1, 1998	11.64	171	61°N-71°N
SPO-2	May 28, 1998	Sept. 17, 1998	11.64	171	82°N-86.3°N 86.3°N-60°N
GCO	Feb. 4, 1999	Feb. 19, 1999	1.97	378-414	60°S-39°S
Mapping	Feb. 20, 1999		1.96	370	90°S

[a]SPO, Science Phasing Orbits: Interim orbits between periods of aerobraking devoted to the collection of science data. GCO, Gravity Calibration Orbit: This period was devoted solely to the collection of highest quality tracking data, and spacecraft disturbances were minimized.

[b]During mapping, MGS is located in a frozen orbit, and periapsis remains over the South Pole [Cutting et al., 1978].

1999, MGS engaged in fixed high-gain antenna mapping operations. In this mode the spacecraft alternately pointed the nadir panel instruments at Mars for 18-20 hrs per day and then the High Gain Antenna (HGA) at the Earth for 4-6 hours per day. Tracking data were collected only when the HGA was pointed at the Earth.

The HGA was deployed on March 29, 1999. After deployment of the High Gain Antenna the nadir panel instruments could point at Mars and collect data while the High Gain Antenna independently tracked the Earth. This mode of operations was used for the remainder of mapping. The only exception was the period of the HGA anomaly from April 15 to May 7, 1999. On April 15, 1999, the azimuth gimbal of the HGA became stuck at 41.5°, causing a 2 week interruption in normal mapping operations, which was followed by ∼1 week of fixed high-gain antenna operations (as in March 1999, but with the boom of the HGA deployed). No data from the period of the HGA anomaly were included in our current geopotential solutions.

Table 1 summarizes the MGS mission phases for which tracking data were included in GMM-2B. No tracking data from the aerobraking mission phases were useful for gravity determination. Although the spacecraft reached altitudes as low as 110-120 km, direct tracking of the spacecraft during the aerobraking passes was not possible because of the configuration of the spacecraft and the relative Earth-Mars geometry. In addition, the spacecraft employed thrusting during the aerobraking pass to maintain attitude, which would contaminate the construction of any orbital arcs longer than one revolution. During SPO-1 and early SPO-2 the High Gain Antenna was not visible during the periapsis passes. Nonetheless, tracking data close to periapsis were still obtained through the low-gain antenna operating in one-way mode on the Radio Science ultrastable oscillator [Lemoine et al., 1999a].

2.2. Data Description

2.2.1. Doppler data.
The MGS spacecraft was tracked by the antennae of the Deep Space Network (DSN) using two-way and three-way ramped Doppler and range. The ramped observable is described by Moyer [1987, 1995]. By two-way we mean the signal is transmitted to MGS, transponded coherently back to the Earth, and received at the transmitting station. In the case of three-way data the signal is transmitted and transponded by MGS in the same fashion: however, the receiving station differs from the transmitting station. Ramped Doppler has been used on previous missions, such as Magellan and Voyager. Ramped Doppler involves a piecewise linear change in the uplink reference frequency and allows the receiving station to lock onto the returned signal more easily. MGS was tracked with unramped Doppler throughout interplanetary cruise to Mars, but tracking switched to ramped Doppler at the start of aerobraking in September 1997.

MGS also collected one-way Doppler data during SPO-1 and SPO-2. In this case the signal originated at the spacecraft from the MGS ultrastable oscillator (USO) [Tyler et al., 1992] and was transmitted via the low-gain antenna (LGA). In this mode, lock-up on the signal from MGS could be achieved earlier than if the data were collected in two-way mode. This was an important consideration in SPO-1 and early SPO-2 as the exit from occultation and the acquisition of signal occurred close to periapsis, and it was important to maximize the quantity of data returned in the vicinity of periapsis.

MGS was tracked primarily by the 34 m High Efficiency Antennae (HEF) of the DSN (stations 15, 45, and 65) and the newer beam-waveguide antennae (BWG) (stations 34, 54, and 25). The averaging times for the X band Doppler data were 60 s in Hiatus and SPO-1 and 10 s for SPO-2 and mapping. The data included in the GMM-2 solutions are summarized in Table 2. The GMM-2A solution included 933,772 Doppler and range observations. The GMM-2B solution included the same Doppler and range observations with no change in the weights applied to normal equations for these tracking data and added the normal equations for 21,343 altimeter crossovers that spanned five arcs in the first 9 months of the mapping orbit.

The ground track coverage is illustrated in Figure 1 for SPO, the Gravity Calibration Orbit (GCO), and mapping.

Table 2. Tracking Data in GMM-2B

Mission Phase[a]	Periapsis Height, km	Number of Arcs	Number of Observations[b]
Hiatus	170	2	24,119
SPO-1	170	8	31,001
SPO-2	170	16	157,972
GCO	370	9	76,813
Mapping	370	47	665,210
Total			955,115

[a]For the purposes of this data summary, Hiatus includes data from October 13 to November 7, 1997; SPO-1 includes data from March 28 to May 1, 1998; SPO-2 includes data from June 1, 1998, to September 17, 1998; GCO includes data from February 5, 1999, through March 13, 1999; and Mapping includes data after deployment of the High Gain Antenna from April 1, 1999, to February 28, 2000.

[b]The MGS mapping data in this table include 21,343 crossovers constructed from the Mars Orbiter Laser Altimeter (MOLA).

Coverage in GCO provided the first global sampling of the planet at low altitude, although there remained some gaps in the longitude coverage and some lack of tracking over the southern polar regions. Tracking later in the mapping phase after deployment of the HGA considerably filled in the areas not well sampled during GCO.

2.2.2. MOLA altimeter and crossover data. The Mars Orbiter Laser Altimeter (MOLA) instrument and experiment summary after the first year of global mapping of Mars are described by *Zuber et al.* [1992] and *Smith et al.* [this issue]. The instrument has a precision of 37.5 cm on flat terrain at normal incidence and operates at a rate of 10 Hz at a wavelength of 1.064 μm. The laser footprint on the surface is ~168 m, depending on the spacecraft altitude, and shots are spaced ~300 m apart. We included a limited set of altimeter crossovers formed from Mars Orbiter Laser Altimeter (MOLA) data in five arcs from March 1999 to December 1999. *Neumann et al.* [this issue] show a technique for using an almost unlimited number of crossovers to refine orbits that have already been determined from conventional tracking. However, that technique requires a parameterization and some approximations that are not appropriate for gravity refinement. In our more rigorous formulation, it is logistically prohibitive to include directly all possible crossovers in the orbit determination analysis since the number of crossovers grows quadratically as $n(n-1)$, where n is the number of

orbits for which altimetry is available. Therefore we selected 21,343 crossovers spanning five arcs in March 1999, May 1999, August 1999, November 1999, and December 1999. These arcs were 5-6 days in length. We included both intra-arc crossovers (crossovers formed from intersecting orbits within a single arc) and inter-arc crossovers (crossovers formed from intersecting orbits that occur in different arcs). The modeling of the crossovers is described by *Rowlands et al.* [1999]. The crossovers were edited for large off nadir pointing angles as well as the slope and roughness of the terrain. No crossovers were included if telemetered external attitude data were unavailable on either orbit track around the crossover. Inter-arc crossovers poleward of 70°N or 70°S were removed to avoid contamination of the MGS orbits by any potential time-varying change in the height of the polar caps. The offsets in orientation of the MOLA instrument with respect to the MGS spacecraft frame determined by *Rowlands et al.* [1999] (-0.0028° in roll and -0.0086° in pitch) were applied.

3. Modeling and Data Analysis

3.1. General Orbit Modeling

The Mars geopotential U is modeled in spherical harmonics using the expression [*Kaula*, 1966]

$$U = \frac{GM}{r}\{1 + \sum_{l=2}^{\infty}(\frac{a_e}{r})^l \sum_{m=0}^{l}[\bar{C}_{lm}\cos m\lambda + \bar{S}_{lm}\sin m\lambda]\bar{P}_{lm}(\sin\phi)\},\tag{1}$$

where G is the universal constant of gravitation, M is the planet mass; a_e is the reference equatorial radius; $\bar{P}_{lm}$ are the normalized associated Legendre functions of degree l and order m; r, λ, and ϕ are the body fixed coordinates of radial distance, longitude, and latitude; and $\bar{C}_{lm}$ and $\bar{S}_{lm}$ are the normalized coefficients of the spherical harmonic expansion. In our analyses the determination of GMM-2B included a solution for the Mars gravitational constant GM and the coefficients $\bar{C}_{lm}$ and $\bar{S}_{lm}$ to degree and order 80. The reference radius was set to 3397.0 km, and the coordinate system was based on the 1991 International Astronomical Union (IAU) system of constants [*Davies et al.*, 1992].

The a priori geopotential model for the normal equations from which GMM-2B was developed was MGM0989C, a preliminary solution to 80 × 80 including MGS data from GCO as well as 3 months of MGS data following deploy-

Figure 1. MGS Doppler tracking coverage in (a) Science Phasing Orbit (SPO), March - September 1998; (b) February and March 1999; and (c) mapping after HGA deployment. The coverage shown in SPO only includes data acquired when the spacecraft was below 500 km altitude. The coverage in SPO was limited to the northern hemisphere owing to the location of periapsis and the eccentricity of the SPO orbit. The data in February and March 1999 (including GCO) provided the first global sampling of the planet from a near-circular low-altitude orbit, although gaps in coverage are still evident at some longitudes and over the southern polar regions. The data in mapping from May 1999 through February 2000 (Figure 1c) fill in gaps not sampled during the first 2 months in the low-altitude mapping orbit.

(a)

(b)

(c)
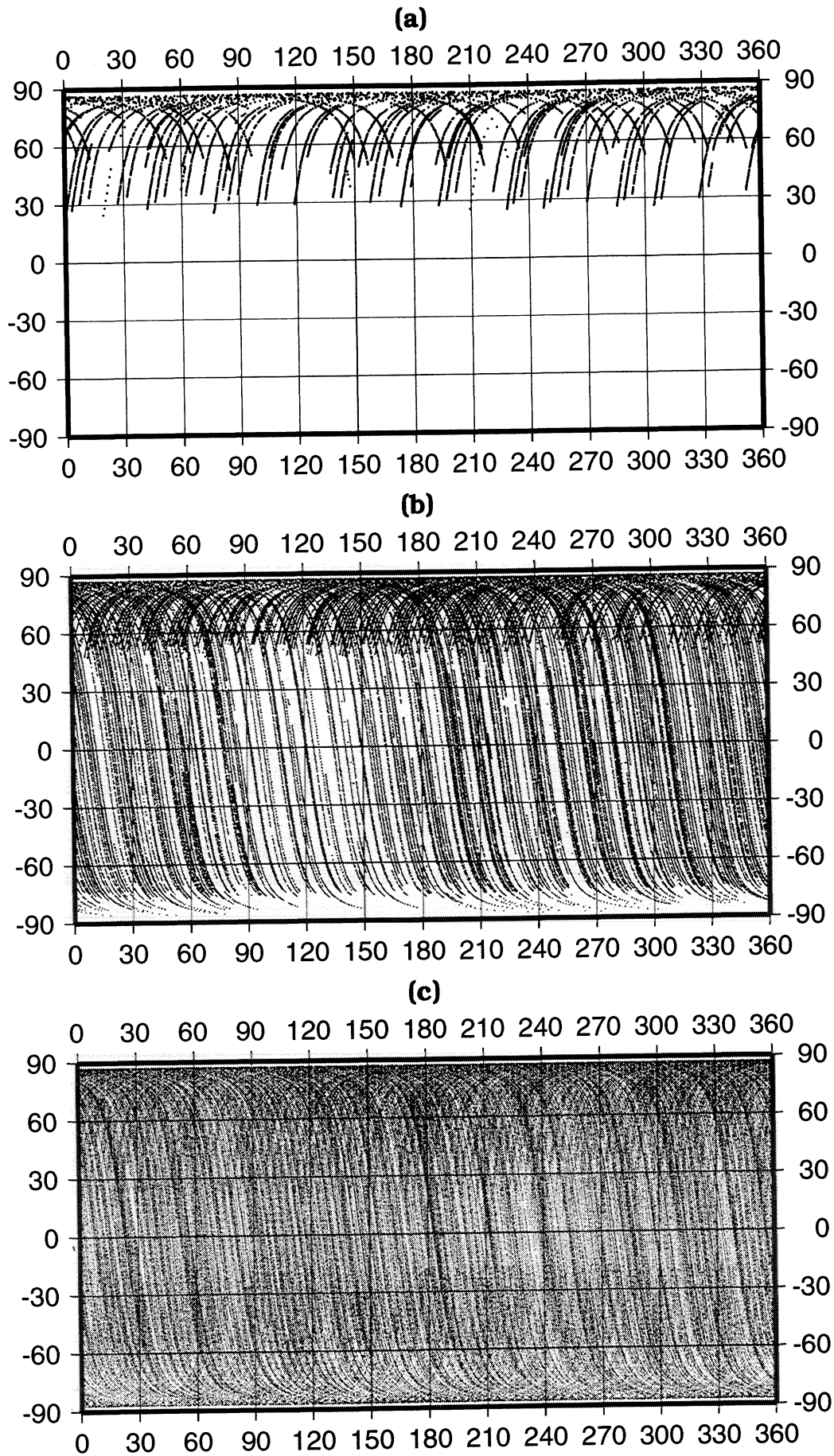
ment of the High Gain Antenna. The GEODYN orbit determination program [*Pavlis et al.,* 2000] was used to process the MGS tracking data. The force and measurement modeling used the DE403 planetary ephemerides [*Standish et al.,* 1995]. The third body accelerations due to the Sun, Moon, planets, and the natural satellites of Mars (Phobos and Deimos) were applied. In addition to the direct solar radiation pressure acting on MGS, the indirect reflected solar radiation from Mars and the radiation pressure from the Mars thermal emission were applied using spherical harmonic models derived from analysis of the Viking Infrared Thermal Mapper data [*Lemoine,* 1992]. It was beyond the scope of this work to sift through the MGS Thermal Emission Spectrometer (TES) data and implement in GEODYN the use of improved models of Mars radiation pressure, although this would be desirable in future analyses. The Stewart atmosphere model was used to compute the atmospheric density at the MGS orbital altitudes [*Stewart,* 1987], and drag coefficients were adjusted in each orbital arc. Future analyses would benefit from the application of improved MGS-derived atmospheric drag models such as those of *Tracadas et al.* [this issue] or Bruinsma and Lemoine (S. Bruinsma, and F. G. Lemoine, A preliminary semi-empirical thermospheric model of Mars: DTM-Mars, submitted to *J. Geophys. Res.,* 2001), although we point out that the adjustment of empirical drag coefficients in an orbital arc can mitigate any errors or differences between atmosphere models at thermospheric altitude.

The Mars solid tide was modeled assuming a k_2 Love number of 0.05. Various relativistic effects are included, including the Schwarzschild effect or the relativistic modification of the central body term in the force model and relativistic light time effects in the measurement model due to the Sun, Jupiter, and Saturn. On MGS the Schwarzschild effect produces an acceleration of 1.3×10^{-9} m/s^2. The relativistic delay on two-way ranges from Earth to Mars ranges from 4 to 37 km for the Sun, 0.9 to 2.7 m for Jupiter, and 0.1 to 0.5 m for Saturn. *Moyer*'s [1981] transformations between coordinate time and atomic time are included by GEODYN in all the interplanetary measurement modeling. The DSN tracking data are corrected for Earth-based tracking station coordinate effects including Earth polar motion, Earth solid tide and ocean loading effects according to *McCarthy,* [1996]. Meteorological data collected at one-half hour intervals at each of the DSN complexes (Goldstone, Madrid, and Canberra) are used to compute an Earth troposphere media correction for the radiometric tracking data.

### 3.2. Angular Momentum Desaturations

MGS periodically fires its thrusters to desaturate its momentum wheels, which absorb angular momentum caused by disturbance torques acting on the spacecraft. During mapping these thruster firings occur autonomously three to four times per day. The attitude control thrusters are designed to fire in pairs so that little or no net velocity impulse is imparted to the spacecraft. However, during these attitude maneuvers, perfect balance between pairs of thrusters

does not occur, and empirical accelerations must be estimated over the duration of each angular momentum desaturation (AMD) event. Each maneuver typically lasts 2-3 min. For the GEODYN processing, constant radial, along-track, and cross-track accelerations are estimated over the duration of each AMD maneuver. On any given day in mapping, failure to account for the AMD maneuvers in the orbit determination analysis can increase the RMS of fit to the Doppler tracking data by several mm/s (10-30 times the nominal data noise). In contrast, during Hiatus and SPO, AMD maneuvers occurred less frequently, and a total of only 29 such events are documented.

3.3. Nonconservative Force Modeling

Proper modeling of the nonconservative forces must account for the complex shape of MGS, the material properties of each surface, and the attitude of the spacecraft and any articulating spacecraft elements. Drawing on similar experience with TOPEX/Poseidon, TDRSS, and GEOSAT Follow-On [*Marshall and Luthcke,* 1994; *Luthcke et al.,* 1997; *Lemoine et al.,* 1999b], MGS is treated as a combination of flat plates arranged in the shape of a box (the spacecraft bus), with attached panels. On the basis of engineering drawings of the spacecraft, a 10 plate model was defined for MGS, including six plates for the spacecraft bus and four plates for the front and back sides of the $+Y$ and $-Y$ panels. The aggregate specular and diffuse reflective properties of each surface are modeled using information supplied by the spacecraft manufacturer, Lockheed Martin (M. Griffin, Lockheed Martin Astronautics, Denver, Colorado, personal communications, January 1999). The $+Y$ and $-Y$ panels are represented as a weighted sum of the area and material properties of the solar array yoke, the inboard GaAs solar array, the outboard Si solar array, and the drag flaps. The solar radiation pressure, Mars reflected solar radiation pressure, the Mars thermal emission, and the atmospheric drag forces acting on each plate are computed and vectorially summed to obtain the total nonconservative force acceleration acting on the MGS spacecraft. Self-shadowing of spacecraft elements is not considered.

The attitude of the MGS spacecraft in inertial space and with respect to Mars is defined in GEODYN using telemetered spacecraft attitude information (quaternions). The processing for each arc requires a continuous stream of quaternion information to define the orientation of the spacecraft in inertial space and to define the orientation of the $+Y$ and $-Y$ panels with respect to the spacecraft body. The quaternions are supplied by the MGS spacecraft team at the Jet Propulsion Laboratory (JPL) and at Lockheed Martin in Denver. Gaps in the quaternion data must be filled prior to processing of any tracking data. Since the general attitude laws of the spacecraft and articulating elements are known, quaternions can be created to fill in any gaps in attitude information. Gaps in attitude information are infrequent after deployment of the High Gain Antenna (with the exception of the period of the High Gain Antenna anomaly, for which we did not process any tracking data). During February and March

GMM-2B to degree 60
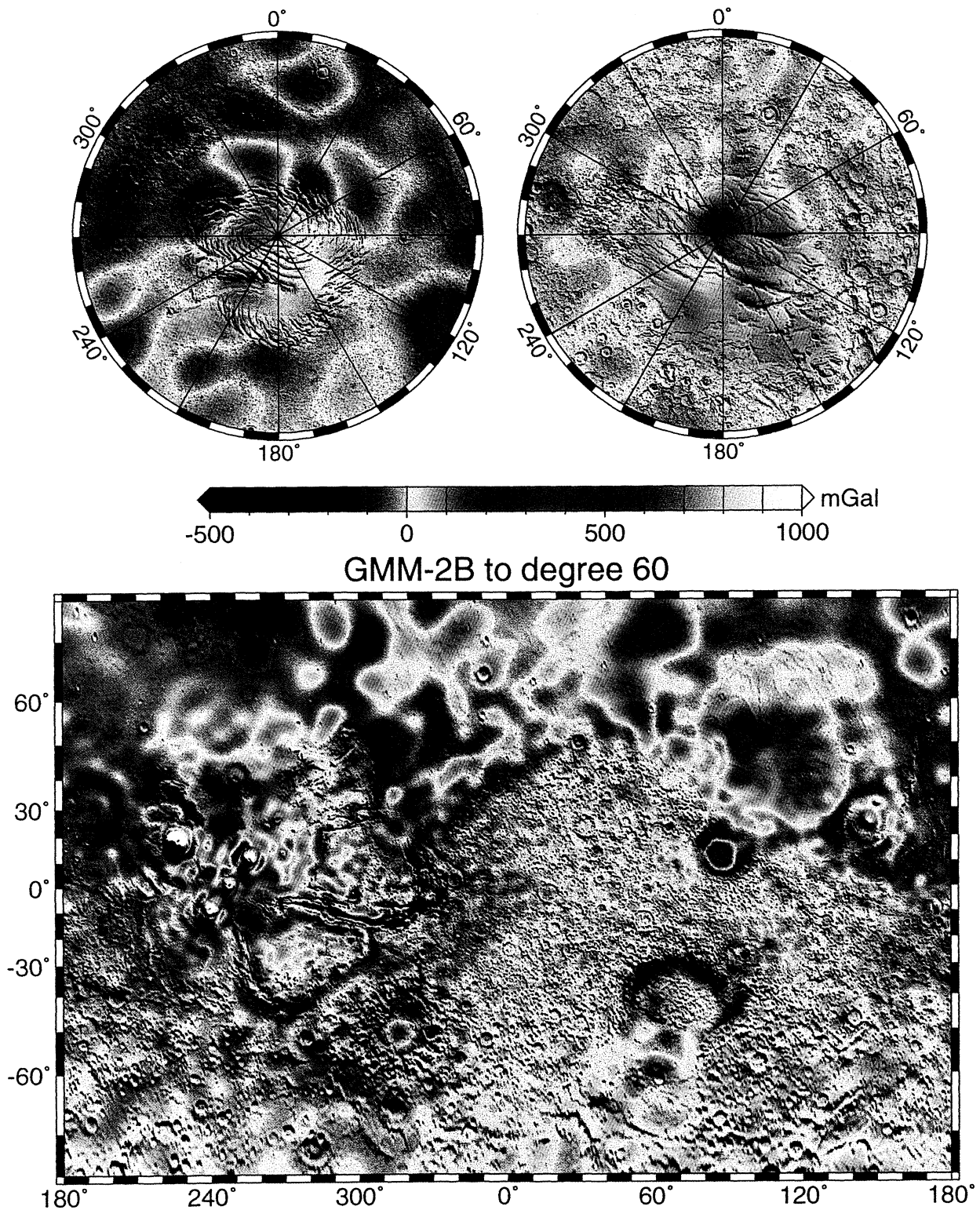
Plate 1. Nonconservative force model accelerations computed using the MGS macromodel on September 24, 1999, at a Mars areocentric solar longitude (L_s) of 211°. The solar radiation pressure acceleration peaks at 8-9 × 10^{-8} m/s^2. The Mars radiation pressure (due to solar radiation reflected from Mars and the planet thermal emission) is of the same magnitude as the atmospheric drag acceleration, although the drag acceleration is primarily along-track, whereas the Mars radiation pressure acceleration is primarily radial.
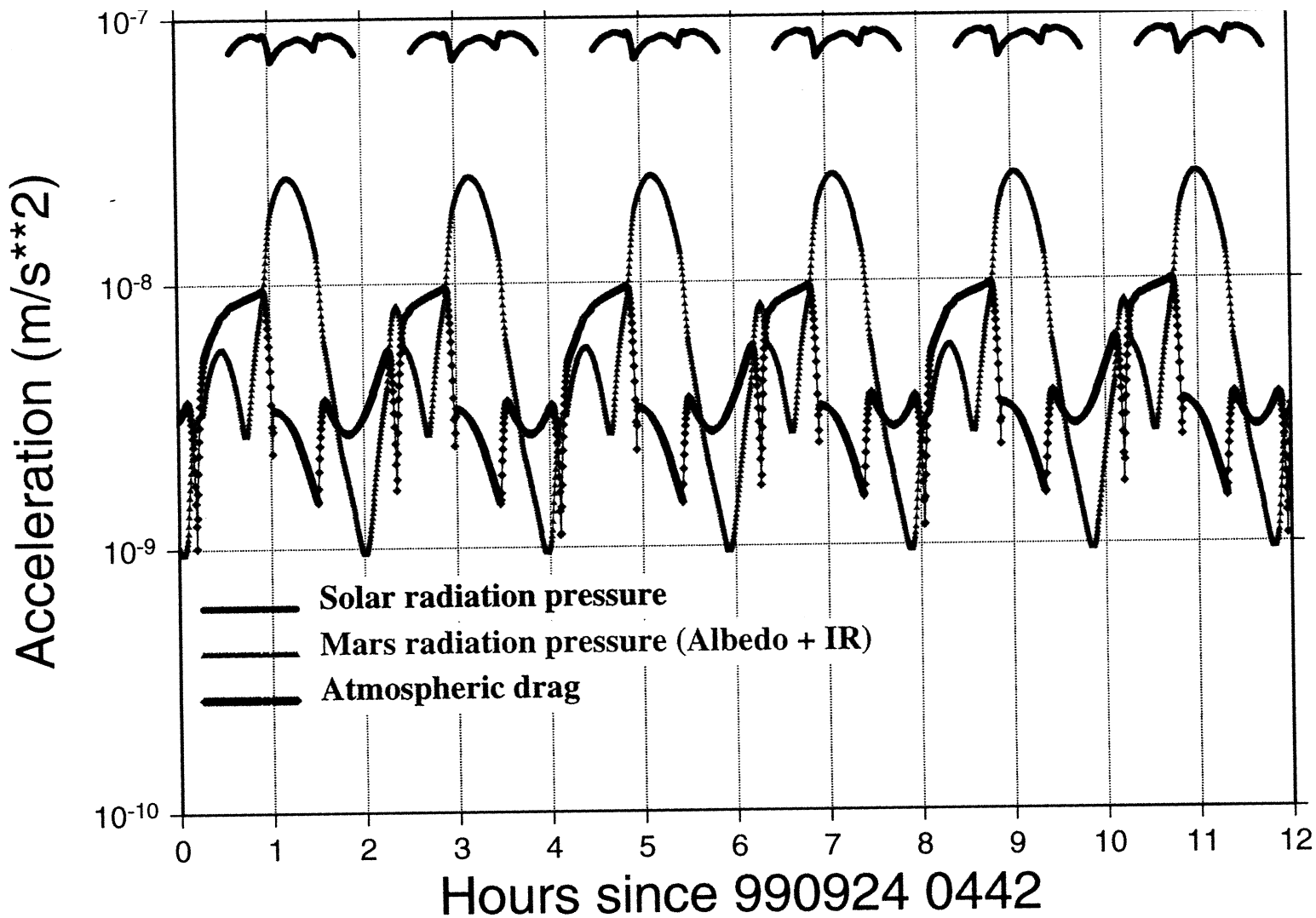
Plate 2. (a) Coefficient and coefficient sigma degree variances of the GMM-1 solution derived from Viking and Mariner 9 tracking and the GMM-2B solution derived from the analysis of the tracking data from Mars Global Surveyor and (b) the coefficient and coefficient sigma degree variances of the model MGM1004E (GMM-2B without the Kaula constraint). The power spectrum of MGM1004E follows the power law curve through degree 60 before increasing in power.

Table 3. MGS Antenna and Center of Mass Offset Corrections

	Coordinates, meters[a]		
	X	Y	Z
HGA (stowed)	0.999	0.000	1.680
LGT1 (stowed)	0.999	-0.716	2.069
LGT2 (stowed)	0.526	-0.763	2.072
LGR1 (+X)	0.806	0.134	0.446
LGR2 (-X)	-0.655	0.000	1.268
CM-(970912)	0.0009	-0.0055	1.3291
CM-(980310)	0.0009	-0.0012	1.2190
CM-(990401)	0.0031	0.0732	0.9534

[a]The coordinates of the HGA and the two transmit LGA in this table apply solely while the HGA was in its stowed configuration. The location of the center of mass is derived from maneuver performance data files supplied by the MGS spacecraft team.

1999, gaps in attitude information were more frequent (from tens of minutes to several hours in length).

Plate 1 depicts the solar radiation pressure, the Mars radiation pressure, and the drag accelerations on MGS for a 12 hour period starting at 11:00 UT on September 24, 1999. The dominant nonconservative acceleration is solar radiation pressure. The average total acceleration is 2.5×10^{-8} m/s^2 for the solar radiation pressure, 4.4×10^{-9} m/s^2 for the Mars radiation pressure, and 2.0×10^{-9} m/s^2 for the atmospheric drag. The Mars radiation pressure peaks in the vicinity of the subsolar point, and the shape of this acceleration curve is driven in part by the strong diurnal contrasts in temperature (100°K or more) between the day and night sides of the planet. The acceleration due to atmospheric drag is a convolution of the density variation with spacecraft altitude and the changing spacecraft cross-sectional area projected in the along-track direction. Since the +Y and -Y panels have a combined surface area of 16 m^2 (compared to areas for the spacecraft body of 2-3 m^2), the changing orientation of the solar arrays plays a large role in the calculation of the nonconservative force accelerations.

3.4. Antenna Offset Modeling

MGS has four low-gain antennae (LGA) and a single high-gain antenna (HGA) [*Semenov,* 1999]. Two low-gain antennae are used for reception (LGR1 and LGR2), and two low gain antennae (LGT1 and LGT2) are used for transmission. The antennae LGR1 and LGR2 are mounted on the +X and -X faces of the spacecraft body. The antennae LGT1 and LGT2 are mounted on a traveling wave tube amplifier box, which itself is mounted on the HGA. The boresight of LGT1 is aligned with the HGA boresight (the +X direction when the HGA was stowed), whereas LGT2 faces the opposite direction (the -X direction when the HGA was stowed). The processing of the tracking data requires that the antenna offsets and motion with respect to the spacecraft center of mass be modeled at all times. Thus an antenna must be associated

uniquely with each pass of tracking data. Most of the two-way and three-way tracking data on MGS in either Hiatus, SPO, GCO, or mapping were transmitted via the HGA. The one-way Doppler data received in SPO were transmitted by LGT1.

The coordinates of the geometric centers of the antennae are summarized in Table 3 in spacecraft body-fixed coordinates. The coordinates of the spacecraft center of mass must also be specified in the same frame, and this information is also provided in Table 3, based on information provided in the MGS instrument kernels. During transitions in attitude regimes in SPO, the antenna offset measurement correction for the LGA Doppler data could reach as high as 0.16 Hz (6 mm/s). In contrast, during attitude regimes when the HGA boresight was pointed at the Earth (for example, generally far from periapsis in SPO and throughout GCO), the antenna offset correction would have no effect on the Doppler data.

After HGA deployment the HGA is located at the end of a 2 m boom, which is extended in the -Z (antinadir) direction. The HGA articulates on two gimbals, one in azimuth and one in elevation to maintain communication with the Earth [*Tyler et al.,* 1992; *Tyler et al.,* this issue; *Semenov,* 1999]. Following *Jaglit* [1998], the HGA offset after deployment can be represented as the sum of two vectors. The first vector, from the origin of the spacecraft coordinate system to a pivot point between the elevation and azimuth gimbals, is fixed in spacecraft coordinates. The second vector is a movable offset that depends on the combined rotation of the azimuth and elevation gimbals. We retrieve the azimuth and elevation angles from MGS telemetry channels and construct quaternions to represent the effect of these combined rotations. GEODYN computes the total HGA antenna offset by summing vectorially the first (fixed) offset and the second (movable) offset at each time step.

3.5. Method of Solution

The tracking data are processed in individual arcs of 12 days length in Hiatus, 4-8 days length in SPO-1 and SPO-2, 1-4 days length in GCO, and 4-6 days length in mapping. In each data arc we adjust the spacecraft state at epoch, drag coefficients (c_d) (a c_d per orbit in Hiatus, a c_d every 12 hours in SPO, a c_d per day in GCO and mapping), a solar radiation pressure reflectivity coefficient per arc, range data biases, frequency biases for the one-way Doppler data, and constant acceleration terms, radial, along-track, and cross-track to the orbit at the times of the angular momentum desaturation maneuvers. Further analysis of the use of spacecraft drag meausurements to determine atmospheric density on Mars is provided by *Tracadas et al.* [this issue].

The MGM0989C solution was already an excellent a priori field, and fits for arcs in mapping with that model that were included in the GMM-2 solutions ranged from 0.0033 Hz to 0.0055 Hz (0.12 to 0.20 mm/s). Compared to the a priori MGM0989C model, the GMM-2 solutions (GMM-2A and GMM-2B) added an extra 5 months of tracking data in mapping (filling in the ground track coverage) and also included more altimeter crossover data.

Normal equations are created on the NASA Goddard Space Flight Center's Cray SV1 processors for each arc and include the common gravity parameters (spherical harmonic coefficients and Mars GM) and the arc-specific parameters. The SOLVE program [*Ullman*, 1997] was used to aggregate the normal equations for each arc and obtain the least squares solution. A Kaula constraint was applied to obtain the GMM-2 solutions; however, compared to the power law used in the GMM-1 solution [*Smith et al.*, 1993], the power law was relaxed and was

$$\sigma_l = \frac{\sqrt{2} \, 13 \times 10^{-5}}{l^2}, \qquad (2)$$

where l is the spherical harmonic degree and σ_l represents the RMS of the coefficient power per spherical harmonic degree, or

$$\sigma_l = \left\{ \frac{1}{2l+1} \sum_{m=0}^{l} (\bar{C}_{lm}^2 + \bar{S}_{lm}^2) \right\}^{1/2}. \qquad (3)$$

In GMM-2B the mapping data were weighted at 0.0047 Hz (0.167 mm/s). The GCO data were weighted at 0.0044 Hz (0.159 mm/s). On the basis of calibrations with subset solutions, the data in SPO and Hiatus were downweighted compared to the mapping orbit data. After application of the various edit criteria, the a priori RMS of fit to the crossover data was 1.9 m. The altimeter crossover data were weighted at 3.2 m in GMM-2B.

We did not include the historic Mariner 9 and Viking Orbiter tracking data in GMM-2B. We tested solutions where the historic data were included and found that the maximum differences in the gravity anomalies of MGS-only and MGS + Viking + Mariner 9 solutions were 5 mGals, with an RMS difference of 0.68 mGal. The RMS difference is much less the predicted error of GMM-2B (11 mGal to degree 60 ×

60). We conclude that the historic data add little, given the superior coverage and precision of the MGS tracking data, although we note that this conclusion is based on the reduction of the 60 s Doppler data at periapsis for the low-altitude Viking orbits. *W.L. Sjogren* (personal communication, 2001) recently reported the recovery of some 10 s Doppler data for the low-altitude Viking orbits.

4. Results

4.1. Degree Variances

The degree variances for the GMM-2B solutions are depicted in Plate 2, (calculated as per equation (3)) and compared to the degree variances from GMM-1 to illustrate the field quality and resolution obtained with the MGS data compared to solutions obtained solely from the historic Viking Orbiter and Mariner 9 data. Whereas for GMM-1 the coefficients had ~100% error by degree 20, with the new MGS-derived field the coefficients do not reach 100% error until degree 60. Below degree 20 the field has been improved by 2-3 orders of magnitude. The coefficient degree variances for GMM-2B without the Mars Kaula constraint (MGM1004E in Plate 2) follow the applied power law to degree 60. Because of a lack of global coverage, GMM-1 was characterized by a dearth of coefficient power beyond degree 20 compared to the Balmino power law for Mars of 13 × $10^{-5}/l^2$ (where l is the spherical harmonic degree). With the global coverage obtained from MGS, the coefficient degree variances do not show such a loss in power even up to degree 80.

Yoder and Standish [1997] and *Smith et al.* [1999a] predict that the normalized annual and semiannual variations in C_{20} and C_{30} will range from 6 to 12 × 10^{-10}. Since the predicted error at degree 2 and degree 3 for GMM-2B is close to 10^{-10}, a detection of these time-varying terms is possible, provided

Table 4. Mars Gravity Anomalies from GMM-1, Mars50c, MGS75D, and GMM-2B[a]

Feature	GMM-1 50 × 50	Mars50c 50 × 50	MGS75D 60 × 60	GMM-2B 50 × 50	GMM-2B 60 × 60
Isidis (85°E, 12°N)	157	197	419	454	411
Elysium (148°E, 25°N)	257	388	754	514	642
Utopia (110°E, 45°N)	132	113	109	109	111
Alba Patera (245°E, 40°N)	361	405	419	420	398
Olympus Mons (226°E, 18°N)	1159	2061	2933	2852	2950
Ascraeus Mons (255°E, 11°N)	538	1179	1689	1413	1728
Pavonis Mons (247°E, 0°N)	400	908	1134	906	1092
Arsia Mons (240°E, 9°S)	586	1339	1619	1353	1526
Argyre (315°E, 50°S)	-48	-107	139	125	137
Valles Marineris					
Noctis Labyrinthus (260°E, 6°S)	135	218	202	186	185
Ius Chasma (287°E, 9°S)	-219	-270	-416	-431	-426
Capri Chasma (312°E, 15°S)	-196	-234	-500	-448	-473

[a]The gravity anomalies were calculated using a Mars rotation rate ω of $7.08821808 \times 10^{-5}$ rad/s, an inverse flattening $1/f$ of 191.2036, and the gravitational constants (GMs) and reference radii (a_e) appropriate to each gravity model. The gravity model GMs are defined in Table 5. The reference radius for the GMM-1, Mars50c, and MGS75D fields is 3394.2 km; the reference radius for the GMM-2B field is 3397.0 km.

North Pole to 60 N   ## South Pole to 60 S
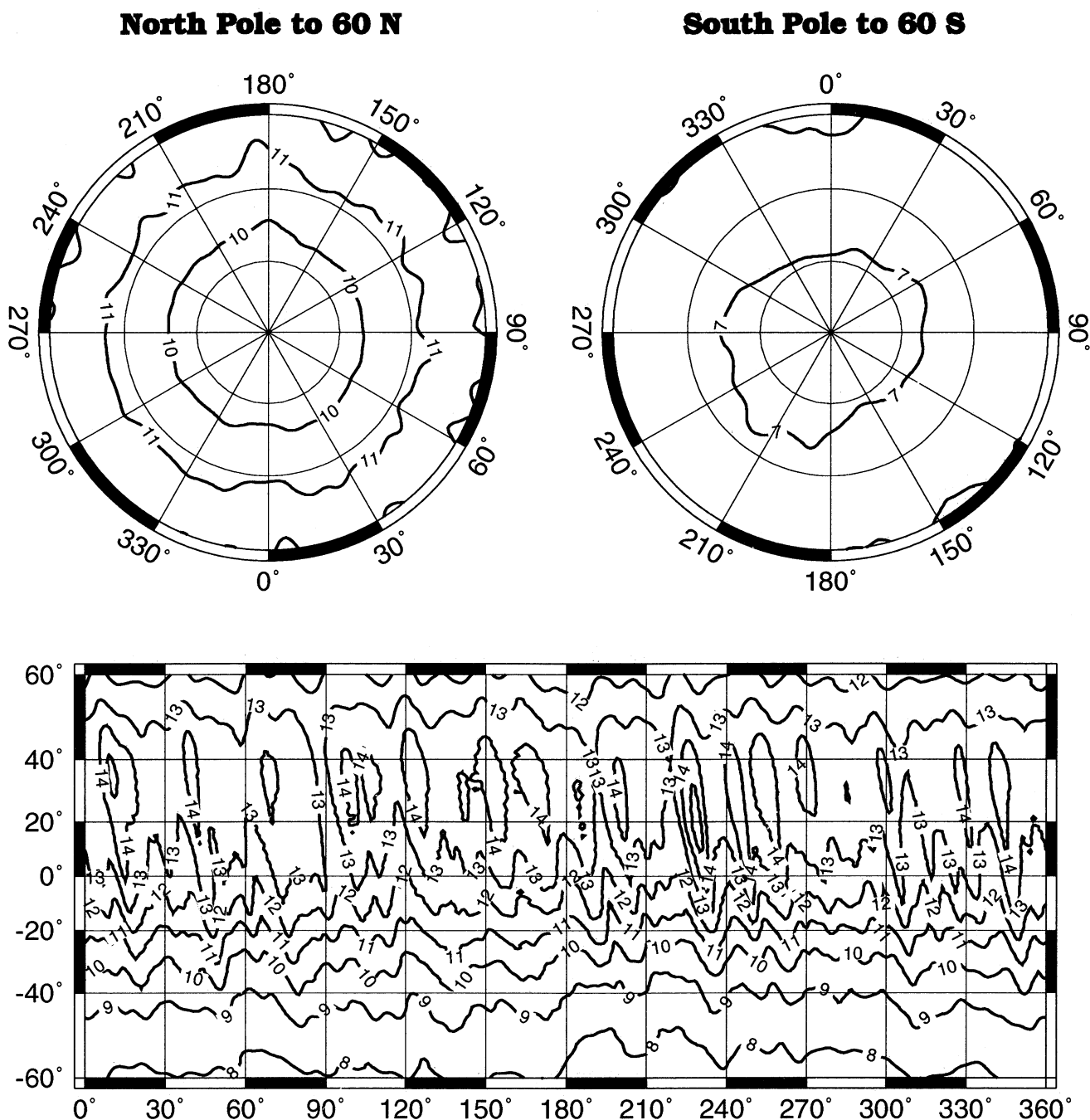
Figure 2. Gravity anomaly error derived from the covariance matrix of the GMM-2B solution evaluated to degree and order 60. The contour interval is 1 mGal. The global RMS error to 60 × 60 is 11 mGal.

sufficient temporal sampling is available from the 400 km mapping orbit.

4.2. Anomalies

The gravity anomalies of the GMM-2B field are depicted in Plate 3. The anomaly map shows the classic features identified in the gravity fields derived from the Viking Orbiter and Mariner 9 tracking, such as Olympus Mons, the Tharsis Montes, Elysium, and Isidis. However, with GMM-2B many of these features now appear with greater power. The anomalies derived from GMM-1 (to 50 × 50) [*Smith et al.*,

1993], Mars50c (to 50 × 50) [*Konopliv and Sjogren*, 1995], MGS75D [*Yuan et al.*, this issue] (to 60 × 60) and GMM-2B (to 50× 50 and 60 × 60) are compared in Table 4.

Valles Marineris appears as a quasi-continuous mass deficit with lows reaching -450 mGals. Olympus Mons is now resolved with an anomaly of 2950 mGals, and the signature of the aureole to the northwest appears distinctly in the gravity anomaly map. Hellas appears as a general low of -50 to -150 mGal with a complicated structure. The muted expression of this feature as a gravity anomaly, compared to its size (1800 km across and 12 km from rim to floor [*Smith et al.*, this

issue]) indicates that it is largely isostatically compensated [*Smith and Zuber*, 1996]. In the northern polar regions several anomalies of -200 to +200 mGals appear between 70°N and 90°N; however, none seem to correlate directly with visible topography or the location of the polar cap. In the southern polar regions a small gravity high of ~100 mGal occurs near the south pole and may correlate with the presence of the polar layered terrains. The power of gravity anomalies in the southern hemisphere appears muted compared to the anomalies in the equatorial regions and the northern hemisphere [*Smith et al.*, 1999b; *Zuber et al.*, 2000]. The most prominent anomaly, situated just south of the Hellas Basin at 62°E, 58°S, is a gravity high of 250 mGal and is associated with Amphitrites Patera, an ancient volcanic shield. Apollinaris Patera, another volcanic shield, is visible in GMM-2B (175°E, 10°S) as a small but prominent gravity high of 225 mGals. This feature was not even discernible in the gravity models derived from the historical Viking and Mariner 9 data. A gravity high of 160 mGal is resolved in the Argyre basin. GMM-2B resolves anomalies of 100-200 mGals in the Utopia basin. Anomalies of that magnitude were already apparent in the GMM-1 and Mars50c fields but did not correlate with topography prior to MOLA [*Zuber et al.*, 2000]. The MGS75D and GMM-2B models are generally comparable over the range of features listed in Table 4, although the MGS75D anomalies are ~100 mGal higher in amplitude over Elysium and Arsia Mons.

4.3. Error Maps

The gravity anomaly errors to 60 × 60, derived from the covariance matrix of the GMM-2B solution, are depicted in Figure 2, so the errors can be compared directly with the gravity anomalies of features listed in Table 4. The commission errors at this degree and order range from 7 to 15 mGals, with a global RMS of 11 mGal. The errors have a generally zonal signature owing to the global tracking coverage and
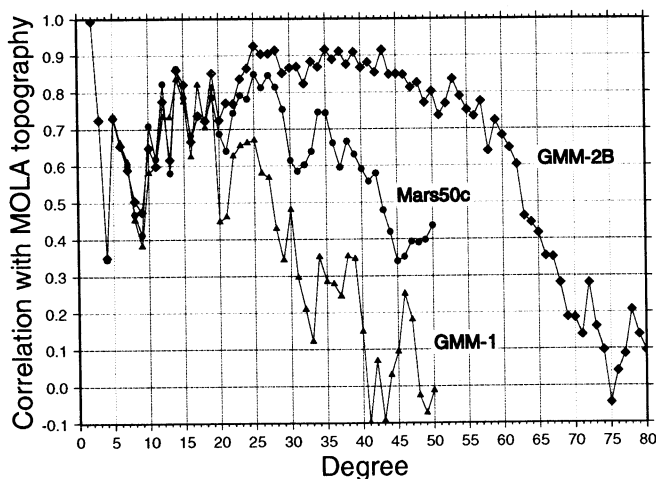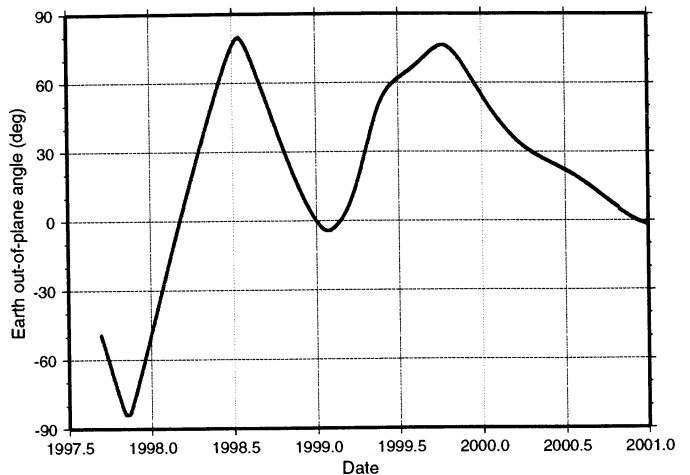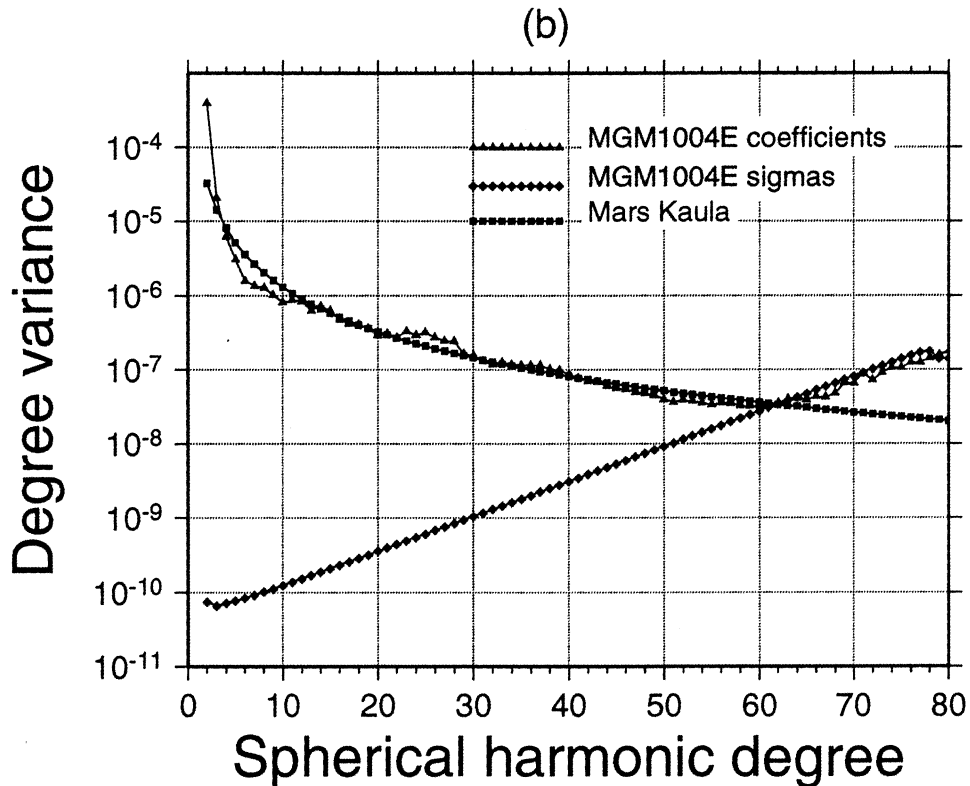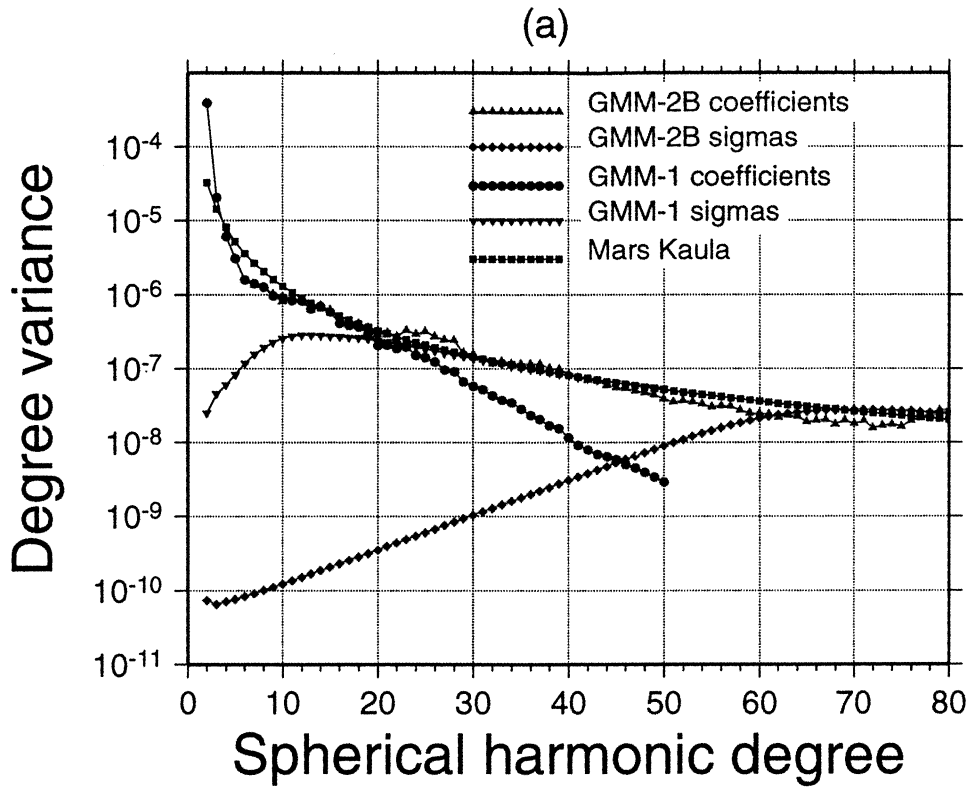

Figure 4. Earth out-of-plane angle for the MGS orbit after orbit insertion through the year 2001. The out-of-plane angle represents the angle between the MGS orbit plane and the line-of-sight with the Earth. An angle of 0° corresponds to edge-on orbit geometry and maximizes the signal in the Doppler data. The Earth out-of-plane angle in GCO ranged from -4° to +2°.

the frozen nature of the spacecraft orbit. The global RMS omission error above degree 60 is ~9 mGal, based on the power law in equation (2) which was applied in the GMM-2B solution (G. Balmino, personal communication, 2000). The minimum error occurs over the southern polar regions (owing to the frozen orbit and the location of periapsis) and is a maximum over the northern mid-latitudes. Errors diminish again at the northern high latitudes because of the convergence of the ground tracks over the polar regions and the impact of the data acquired in SPO when periapsis was at 170 km. Figure 2 also shows some longitudinal variations (1-2 mGal) in the predicted gravity anomaly error which may be attributed to variations in the density and sensitivity of the tracking data used in the GMM-2B solution.

The geoid errors mapped from the covariance matrix of the GMM-2B solution have essentially the same quasi-zonal signature as the error map of the gravity anomalies. Through 60×60 the predicted geoid error ranges from 1.0 to 2.6 m with a global RMS of 1.8 m.

4.4. Correlation With Topography

GMM-2B may also be evaluated by computing the global correlation by degree between the planetary shape as determined by the MOLA instrument and the gravity coefficients. The correlations were computed using a spherical harmonic expansion of the topography to degree and order 90. The global correlations computed from the spherical harmonic coefficients of the Mars50c, GMM-1, and GMM-2B fields with coefficients from a Mars topography solution derived from the MOLA altimeter data are illustrated in Figure 3. The average global correlations to degree 50 are 0.43 for GMM-1, 0.64 for Mars50c, and 0.79 for GMM-2B. The correlation remains above 0.6 through degree 62, after which there is a sharp dropoff in signal. The sharp decline in cor-

Figure 3. Correlation coefficients between the indicated gravity models (GMM-1, Mars50c, and GMM-2B) with a spherical harmonic shape model determined from MOLA data. The global correlation to degree 60 for GMM-2B is 0.78.

(a)

(b)

Plate 3. Gravity anomalies of the GMM-2B solution evaluated to 60 × 60. The anomalies are evaluated using the following constants: $GM = 4.2828371901 \times 10^{13}$ m³/s², reference radius a_e of 3397000.0 meters; rotation rate ω of $7.08821808 \times 10^{-5}$ rad/sec; and an inverse flattening $1/f$ of 191.2036. This analysis uses areocentric coordinates with an east positive longitude convention. The gravity anomalies are shown on a Mercator projection to ± 75° latitude, and on polar stereographic projections to 70°N for the northern polar projection (upper left figure), and to 70°S for the southern polar projection (upper right figure). The gravity anomalies are overlain on a shaded relief map of the martian topography determined from MOLA data.

Table 5. Determinations of the Mars *GM*

Data	GM, km^3/s^2	Source
Mariner 4 flyby	42828.32 ± 0.13	*Null* [1969]
Mariner 6 flyby	42828.22 ± 1.83	*Anderson et al.* [1970]
Mariner 9 hyperbolic approach	42828.35 ± 0.55	*O'Neil et al.* [1973]
Mariner 9 observations of Phobos and Deimos	42828.1 ± 0.5	*Born* [1974]
GMM-1	42828.3580 ± 0.0512	*Smith et al.* [1993]
Mars50c	42828.370371 ± 0.001	*Konopliv and Sjogren* [1995]
MGS75D	42828.382332 ± 0.000077	*Yuan et al.* [this issue]
GMM-2B	42828.371901 ± 0.000074	this paper

relation above degree 62 is due to the decline in power of the gravity field coefficients, which is caused by the limit of MGS tracking data sensitivity.

4.5. GM Solutions

In Table 5 we compare various solutions for *GM* and their formal standard deviations. For many years the estimate determined by *Null* [1969] was the best determined value because of its unusually tight standard deviation. The GMM-2B value is in close agreement with Mars50c solution but differs by two parts in 10^7 from the value determined with MGS75D [*Yuan et al.* this issue]. The MGS75D *GM* estimate may be an outlier as a later solution by the same authors that includes more MGS mapping data, MGS75E, yields a *GM* estimate of 42828.377 km^3/s^2 (D.-N. Yuan, personal communication, 2001).

The tight formal standard deviation on the Mars *GM* in the MGS solutions results from the GCO data, which have unusual strength because of highly favorable viewing geometry and the near-continuous tracking. Figure 4 depicts the

Table 6. Orbit Overlaps in the Gravity Calibration Orbit

Gravity Field[a]	Average Orbit Overlaps, meters[b]			
	Radial	Cross-track	Along-track	Total
MGM0964C18	0.28	75.50	2.31	75.57
MGS75B	0.23	68.61	3.09	68.71
MGS75D	0.58	35.75	1.59	35.85
GMM-2A	0.08	12.30	0.56	12.32
GMM-2B	0.05	5.64	0.27	5.66

[a]The MGM0964C18 solution to 70x70 from *Smith et al.* [1999b] and the MGS75B solution to 75 × 75 from *Sjogren et al.* [1999] are based on 2 months of MGS data after arrival in the mapping orbit and prior to deployment of the High Gain Antenna. The MGS75D [*Yuan et al.*, this issue], solution to 75 × 75 based on MGS data through March 27, 2000. The GMM-2A solution (to 80 × 80) includes MGS mapping data through February 29, 2000, but no altimeter crossover data. GMM-2B, also to 80 × 80, contains the same tracking data as GMM-2A and adds the MOLA altimeter crossover data.

[b]These orbit tests consist of 12 overlaps of 13 arcs from February 5, 1999, to February 24, 1999. The arcs are exactly 30 hours in length, and the overlaps between adjacent arcs are 6 hours.

out-of-plane angle for the MGS orbit with respect to the line of sight with the Earth. An angle of 0° corresponds to an edge-on orbit geometry, and an angle of 90° corresponds to a face-on orbit geometry. Between February 5, 1999, and March 1, 1999, the orbit out-of-plane angle ranged from -4° to +2°. An edge-on viewing geometry maximizes the orbital velocity signal observed by the Doppler data. In contrast, for the bulk of the period after the deployment of the High Gain Antenna for which data were included in GMM-2B, the out-of-plane angle was above 40°, and from June through December 1999, the out-of-plane angle was above 60°, resulting in diminished Doppler sensitivity. The sensitivity of the remaining mapping data to the Mars *GM* is 100 times smaller than the sensitivity of the GCO data.
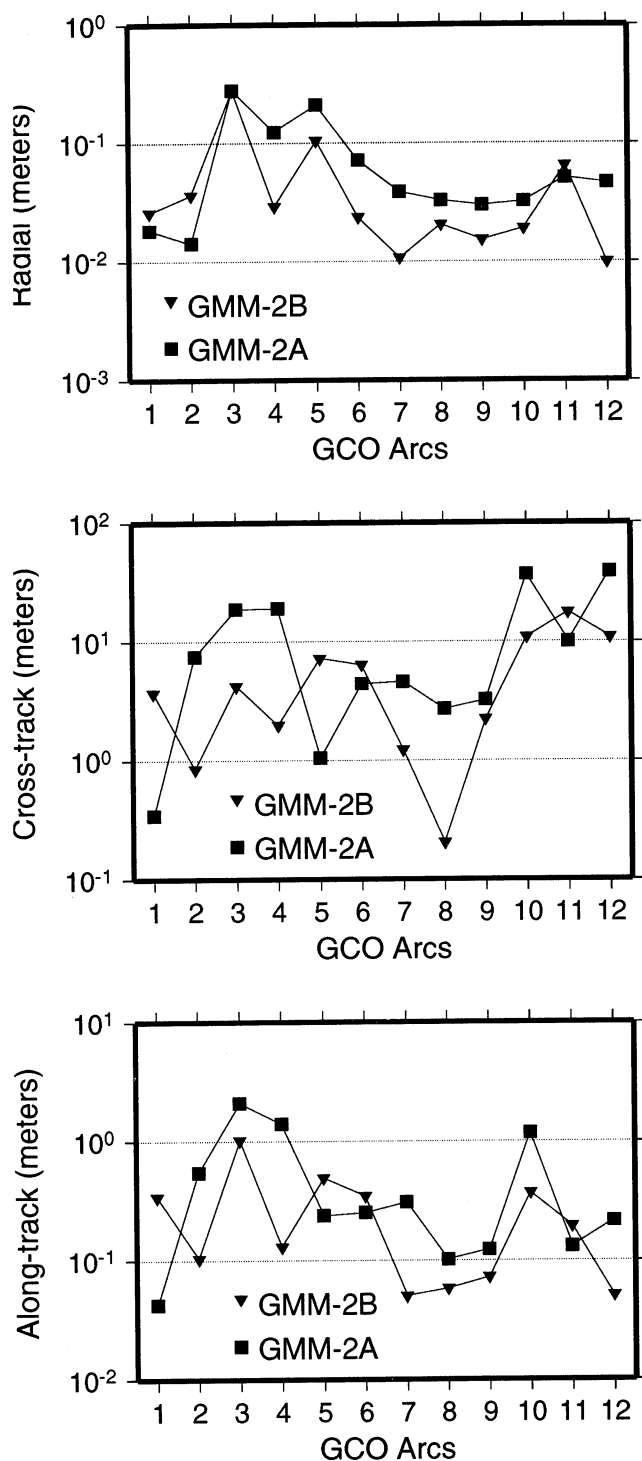
4.6. Orbit Results

We may evaluate the GMM-2 solutions by computing the differences in orbital position from arcs that share a common time span. The first test case involved 13 arcs in GCO from February 6 to February 23, 1999. The arcs were 30 hours in length and overlapped by 6 hours. The data in GCO are the most suitable for testing subtle differences in orbit performance because of the near-continuous tracking coverage and because the spacecraft was maintained in a quiescent state in order to minimize any disturbances in the tracking data. The HGA was undeployed, and by design the HGA boresight was pointed continuously at the Earth to eliminate the effect of antenna motion in the Doppler data. The results are reported in Table 6 for GMM-2A (the companion model to GMM-2B that does not include the MOLA altimeter crossover data) and GMM-2B (which includes the MOLA crossover data). The results are also shown for two preliminary MGS solutions, MGM0964C18 and MGS75B, based on two months of MGS data following arrival in the mapping orbit [*Smith et al.*, 1999b], as well as MGS75D, a 75 × 75 solution from *Yuan et al.*, [this issue] based on MGS data through March 27, 2000. For these tests we compute the average orbit overlap per component using the set of 12 orbit overlaps. For GMM-2B in the radial direction, we have an average orbit consistency of under a decimeter in the radial direction and 5.7 m in total position. That the orbit is more poorly determined in the cross-track direction is consistent with the MGS edge-on orbit plane geometry of the gravity calibration orbit.

Figure 5. Expansion of the orbit overlaps for the gravity calibration orbit (GCO) test arcs presented in Table 6 for GMM-2A (solution without the altimeter crossover data) and GMM-2B (solution with the altimeter crossover data).

A comparison of the GMM-2A and GMM-2B solutions reveals that the altimeter crossover data contribute some enhanced sensitivity to the low-degree odd zonal harmonics, to the high-degree zonals above degree 50, and to a high-order resonance near order 62. The change in the calculated value of the gravity anomalies due to the addition of the altimeter

crossover data is negligible (< 0.1 mGal). Nevertheless, the orbit tests do provide some evidence that the addition of the MOLA altimeter crossovers strengthens the gravity solution, since the total orbit discrepancy is reduced from 12.3 to 5.7 m. The orbit overlap improvement occurs for 8 of the 12 test arcs, as illustrated in Figure 5.

The GMM-2B gravity solution was also evaluated using a second series of orbits after HGA deployment. A total 47 overlaps of 52 arcs from April 2, 1999, to December 27, 1999, were used. The arcs were 5-6 days in length and overlapped by 12-24 hours. The results are summarized in Table 7. The orbit overlaps for GMM-2B in the radial direction are noticeably higher than for the tests done with data in GCO. We obtain radial orbit overlaps of on average 1 m compared to an average better than 10 cm in GCO. A number of factors may be responsible for the higher overlaps including longer arc length, less favorable orbit geometry with respect to the Earth line-of-sight, and more frequent gaps in tracking. In these tests we do not discern any change due to the addition of the altimeter crossover data in GMM-2B compared to GMM-2A. The differences in performance between the preliminary MGS solutions (MGM0964C18 and MGS75B), MGS75D, and the GMM-2 solutions may be explained largely by the increased amount of tracking data in the GMM-2 solutions.

4.7. Fit to Historical Data

We also evaluated GMM-2B by computing its fit to the historical Mariner 9 and Viking Orbiter data. For GMM-2B these data are independent, since the historical data were not included in the gravity solution. The RMS of fit for Viking and Mariner 9 is compared in Table 8 with results obtained from the models GMM-1 [*Smith et al.,* 1993] and Mars50c [*Konopliv and Sjogren,* 1995], which were models determined solely from the historical data. The RMS is computed separately for each distinct spacecraft orbit type for both the Doppler and the range data so we can compare the performance for different orbit geometries.

With the exception of some deeply resonant Viking orbits with a periapsis altitude of 1500 km, the MGS-only derived field, GMM-2B, fits the historical Mariner 9 and Viking Or-

Table 7. Orbit Overlaps in After HGA Deployment

Gravity Field	Average Orbit Overlaps, m[a]			
	Radial	Cross-Track	Along-Track	Total
MGM0964C18	2.53	32.01	97.19	103.72
MGS75B	2.58	27.24	81.61	86.93
MGS75D	1.17	4.77	13.98	15.18
GMM-2A	1.02	2.56	8.69	9.34
GMM-2B	1.05	2.55	8.75	9.38

[a]In these orbit comparisons, 47 overlaps of 52 arcs from April 2, 1999, to December 27, 1999 (after deployment of the HGA), were used. The average arc length was 6.06 days, and the average period of overlap between adjacent arcs was 1.25 days.

Table 8. Gravity Model RMS of fit to Mariner 9 and Viking Orbiter Tracking Data

Spacecraft	Periapsis Height, km	Number of Arcs	Data[a]	Gravity Models		
				GMM-1	Mars50c	GMM-2B
Mariner 9	1600	51	Doppler	1.05	1.04	1.01
Viking-1	1500	31	Doppler	1.89	1.88	2.58
		21	Range	11.54	11.48	14.76
Viking-2	1500	23	Doppler	2.64	2.61	2.60
		12	Range	6.38	4.85	5.59
Viking-2	800	49	Doppler	0.99	0.76	0.94
		40	Range	5.74	4.53	5.11
Viking-1	300	95	Doppler	1.96	1.27	1.03
		30	Range	5.55	4.04	2.38
Viking-2	300	29	Doppler	1.86	3.17	0.99
		2	Range	3.72	1.51	1.77

[a]The RMS of fit is in mm/s for the Doppler data and meters for the range data.

biter data at the same level or better than the fields that actually included these historical data. The data from the 300 km periapsis orbits of Viking Orbiter 1 and Viking Orbiter 2 fit GMM-2B better than the other gravity models that actually include these data and provide some interesting validation of the accuracy of the MGS-derived gravity field. It is only the Viking-1 1500 km periapse data that show a higher RMS of fit with GMM-2B. The higher RMS of fit may be attributed to deep resonance effects on this Viking orbit. For several months after deployment of the Viking-1 Lander (VL-1), the Viking-1 Orbiter was maintained in a 1500 km periapse orbit that overflew the VL-1 site once per Mars day [*Snyder*, 1977]. By definition, this produces an orbit in deep resonance, which the gravity model based only on MGS data does not handle as well as the GMM-1 and Mars50c fields, which actually included tracking data from this resonant orbit.

5. Summary and Conclusions

We have developed a new model of the Mars gravity field in spherical harmonics to degree and order 80 using tracking data to Mars Global Surveyor and altimeter crossovers formed from the Mars Orbiter Laser Altimeter (MOLA).

Although various results (see the degree variances and the correlations with topography) would on the surface suggest that in a global sense the model is of high fidelity only through degree 60, we are not justified in solving only for coefficients through degree 60 primarily because of aliasing effects. The MGS data have sensitivity to numerous features (e.g., the Tharsis Montes or Amphitrites Patera) that have dimensions of only a few degrees. Truncating the solution at only at degree 60 would mean folding back their signal into the lower degrees. Because of these aliasing effects, the 60 × 60 version of GMM2B (MGM1004I) degrades the orbit quality as measured by the GCO test arcs. Referring to Table 6, the equivalent average orbit overlaps of MGM1004I are 0.18 m radially, 25.36 m cross-track, 1.14 m along-track, and 25.41 m in total position, representing a factor of 5 degra-

dation in orbit quality compared to the 80 × 80 GMM-2B solution.

Because of the near-circular orbit at a mean altitude of 400 km and the quality of the X band tracking system, the new model, determined solely from the MGS data, is a significant improvement over models determined earlier from only the Viking Orbiter and the Mariner 9 tracking data. The resolution of numerous features such as the Tharsis volcanos, Isidis, and Elysium, is improved, and in addition, new features have been identified in the gravity anomaly maps. The model in a global sense can be used confidently for geophysical interpretation through degree 60, although locally the resolution may be superior. A spatial and spectral localization analysis of the type performed by *Simons et al.* [1997] would be useful to evaluate the information content of the GMM2B model.

Further improvements in Mars gravity field modeling can be anticipated with the addition of data from the remainder of the mission (after February 2000). The additional data will provide increased resolution and better sensitivity to gravitational perturbations, as the orbit out-of-plane angle becomes edge-on in late 2000.

References

Anderson, J. D., L. Efron, and S. K. Wong, Martian mass and Earth-Moon mass ratio from coherent S-band tracking of Mariners 6 and 7, *Science, 167,* 277-279, 1970.

Ash, M. E., I. I. Shapiro, and W. B. Smith, Astronomical constants and planetary ephemerides deduced from radar and optical observations, *Astron. J., 72,* 338-350, 1967.

Balmino, G., B. Moynot, and N. Valès, Gravity field of Mars in spherical harmonics up to degree and order eighteen, *J. Geophys. Res., 87,* 9735-9746, 1982.

Born, G. H., Mars physical parameters as determined from Mariner 9 observations of the natural satellites and doppler tracking, *J. Geophys. Res., 79*(32), 4837-4844, 1974.

Christensen, E. J., and G. Balmino, Development and analysis of a twelfth Degree and Order gravity model for Mars, *J. Geophys. Res., 84*(B14), 7943-7953, 1979.

Christensen, E. J., and B. G. Williams, Mars gravity field derived from Viking-1 and Viking-2: The navigation result, *J. Guidance and Control 2*(3), 179-183, 1979.

Cutting, E., G. H. Born, and J. C. Frautnick, Orbit Analysis for SEASAT-A, *J. Astron. Sci., 26,* 315-342, 1978.

Davies, M. E., et al., Report of the IAU/IAG/COSPAR working group on cartographic coordinates and rotational elements of the planets and satellites: 1991, *Celestial Mech. Dyn. Astron., 53,* 377-397, 1992.

Esposito, P., V. Alwar, S. Demcak, E. Graat, M. Johnston, and R. Mase, Mars Global Surveyor navigation and aerobraking at Mars, *AAS Paper 98-384,* paper presented at AAS/AIAA Space Flight Mechanics meeting, Monterey, Calif., Feb. 9-11, 1998.

Gapcynski, J. P., R. H. Tolson, and W. H. Michael, Jr., Mars gravity field: Combined Viking and Mariner 9 results, *J. Geophys. Res., 82*(28), 4325-4327, 1977.

Jaglit, M., Spacecraft HGA phase center and line of boresight movements after deployment with azimuth and elevation gimbal positions, *Interoff. Memo. 98-011,* Lockheed Martin, Denver, Colo., Feb. 16, 1998.

Johnston, M. D., P. B. Esposito, V. Alwar, S. W. Demcak, E. J. Graat, P. D. Burkhart, and B. M. Portock, The strategy for the second phase of aerobraking Mars Global Surveyor, *AAS Paper 99-303,* paper presented at AAS/AIAA Astrodynamics Specialist Conference, Girdwood, Alaska, Aug. 16-19, 1999.

Kaula, W. M., *Theory of Satellite Geodesy,* Blaisdell, Waltham, Mass., 1966.

Konopliv, A. S., and W. L. Sjogren, The JPL Mars gravity field, Mars50c, based upon Viking and Mariner 9 Doppler tracking data, *JPL Publ. 95-5,* Jet Propul. Lab., Pasadena, Calif., Feb. 1995.

Lemoine, F. G., The dynamics of orbiting satellites and gravity model development, Ph.D thesis, 413 pp, Univ. of Colo., Boulder, Colo., 1992.

Lemoine, F. G., D. D. Rowlands, G. A. Neumann, D. E. Smith, D. E. Pavlis, D. S. Chinn, and S. B. Luthcke, Precise orbit determination for Mars Global Surveyor during Hiatus and SPO, in *Spaceflight Mechanics 1999, Advances in the Astronautical Sciences,* vol. 102, edited by R. H. Bishop, et al., pp. 649-665, Univelt Inc., San Diego, Calif., 1999a.

Lemoine, F. G., D. D. Rowlands, N. P. Zelensky, S. B. Luthcke, C. M. Cox, and G. C. Marr, Precise orbit determination for the GEOSAT-follow-on spacecraft, in *1999 Flight Mechanics Symposium, NASA Conf. Publ., NASA/CP-1999-209235,* Greenbelt, Md., 495-508, 1999b.

Lorell, J., et al., Gravity field of Mars from Mariner 9 tracking data, *Icarus, 18,* 304-316, 1973.

Luthcke, S. B., J. A. Marshall, S. C. Rowton, K. E. Rachlin, C. M. Cox, and R. G. Williamson, Enhanced radiative force modeling of the Tracking and Data Relay Satellites, *J. Astron. Sci., 45*(3), 349-370, 1997.

Marshall, J. A. M., and S. B. Luthcke, Radiative force model performance for TOPEX/Poseidon precision orbit determination, *J. Astron. Sci., 45*(2), 229-246, 1994.

McCarthy, D. D. (Ed.), *IERS Conventions (1996),* IERS Tech. Note 21, U.S. Naval Obs., Washington D. C., 1996.

Moyer, T. D., Transformation from proper time on Earth to coordinate time in solar system barycentric space-time frame of reference, part I and part II, *Celestial Mech., 23,* 33-68, 1981.

Moyer, T. D., Changes to the ODF and ODE for processing X-band uplink data, *Eng. Memo., 314, 4-430,* Jet Propul. Lab., Pasadena, Calif., 1987.

Moyer, T. D., REGRES modifications for processing Block V exciter range observables, *Eng. Memo., 314, 5-1795,* Jet Propul. Lab., Pasadena, Calif., 1995.

Neumann, G. A., D. D. Rowlands, F. G. Lemoine, D. E. Smith, and M. T. Zuber, The crossover analysis of Mars Orbiter Laser Altimeter data, *J. Geophys. Res.,* this issue.

Null, G. W., A solution for the mass and dynamical oblateness of Mars using Mariner-IV Doppler data, *Bull. Am. Astron. Soc., 1,* 356, 1969.

O'Neil, W. J., et al., Mariner 9 navigation, *Technical report 32-1586,* Jet Propul. Lab., Pasadena, Calif., Nov. 1973.

Pavlis, D. E., S. G. Poulose, S. C. Rowton, J. J. McCarthy, and S. B. Luthcke, GEODYN operations manuals, contractor report Raytheon ITSS, Greenbelt, Maryland, March 15, 2000.

Reasenberg, R. D., I. I. Shapiro, and R. D. White, The gravity field of Mars, *Geophys. Res. Lett., 2*(3), 89-92, March 1975.

Rowlands, D. D., D. E. Pavlis, F. G. Lemoine, G. A. Neumann, and S. B. Luthcke, The use of laser altimetry in the orbit and attitude determination of Mars Global Surveyor, *Geophys. Res. Lett., 26,* 1191-1194, 1999.

Semenov, B., MGS Antenna Frames SPICE instrument kernel (version 1.0), Jet Propul. Lab., Pasadena, Calif., March 1, 1999.

Simons, M., S. C. Solomon, and B. H. Hager, Localization of gravity and topography constraints in tectonics in mantle dynamics of Venus, *Geophys. J. Int., 131*(1), 24-44, 1997.

Sinclair, A. T., The motions of the satellites of Mars, *Mon. Not. R. Astron. Soc., 155,* 249-274, 1972.

Sjogren, W. L., Mars gravity: High resolution results from Viking Orbiter 2, *Science, 203,* 1006-1010, 1979.

Sjogren, W. L., J. Lorell, L. Wong, and W. Downs, Mars gravity field based on a short-arc technique, *J. Geophys. Res., 80,* 2899-2908, 1975.

Sjogren, W. L., R. N. Wimberly, D. L. Cain, and J. P. Brenkle, Mars gravity: Additional resolution from Viking Orbiter 1, in *Proceedings of the Lunar and Planetary Science Conference,* pp. 3561-3573, Pergamon, New York, 1978.

Sjogren, W. L., D.-N. Yuan, and A. S. Konopliv, Mars gravity field modeling with MGS, Spring meeting, *Eos Trans. AGU, , 80*(17), Suppl., S204, 1999.

Smith, D. E., and M. T. Zuber, The shape of Mars and the topographic signature of the hemispheric dichotomy, *Science 271,* 184-188, 1996.

Smith, D. E., F. J. Lerch, R. S. Nerem, M. T. Zuber, G. B. Patel, S. K. Fricke, and F. G. Lemoine, An improved gravity model for Mars: Goddard Mars Model 1, *J. Geophys. Res., 98*(E11), 20871-20889, 1993.

Smith, D. E., M. T. Zuber, R. M. Haberle, D. D. Rowlands, and J. R. Murphy, The Mars seasonal CO_2 cycle and the time variation of the gravity field: A general circulation model simulation, *J. Geophys. Res., 104,* 1885-1896, 1999a.

Smith, D. E., W. L. Sjogren, G. L. Tyler, G. Balmino, F. G. Lemoine, and A. S. Konopliv, The gravity field of Mars: Results from Mars Global Surveyor, *Science, 286,* 94-97, 1999b.

Smith, D. E., et al., Mars Orbiter Laser Altimeter (MOLA): Experiment summary after the first year of global mapping of Mars, *J. Geophys. Res.,* this issue.

Snyder, C. W., The missions of the Viking Orbiters, *J. Geophys. Res., 82*(28), 3971-3983, 1977.

Snyder, C. W., The extended mission of Viking, *J. Geophys. Res.,* *84*(B14), 7917-7933, 1979.

Standish, M. E., X X Newhall, J. G. Williams, and W. M. Folkner, JPL planetary and lunar ephemerides DE403 /LE403, *JPL Interoff. Memo. 314.10-127,* Jet Propul. Lab., Pasadena, Calif., May 22, 1995.

Stewart, A. I. F., Revised time dependent model of the martian atmosphere for use in orbit lifetime and sustenance studies, final report, JPL PO NQ-802429, Lab. for Atmos. and Space Phys., Univ. of Colorado, Boulder, March 26, 1987.

Tracadas, P., M. T. Zuber, D. E. Smith, and F. G. Lemoine, Density structure of the upper thermosphere of Mars from measurements of air drag on the Mars Global Surveyor spacecraft, *J. Geophys. Res.,* this issue.

Tyler, G. L., G. Balmino, D. P. Hinson, W. L. Sjogren, D. E. Smith, R. Woo, S. W. Asmar, M. J. Connally, C. L. Hamilton, and R. A. Simpson, Radio science investigations with Mars Observer, *J. Geophys. Res., 97,* 7759-7779, 1992.

Tyler, G. L., G. Balmino, D. P. Hinson, W. L. Sjogren, D. E. Smith, R. A. Simpson, S. W. Asmar, P. Priest, and J. D. Twicken, Radio science observations with Mars Global Surveyor: orbit insertion through one year in mapping orbit, *J. Geophys. Res.,* this issue.

Ullman, R., SOLVE program mathematical formulation, *Rep. HSTX-G & G-9201,* Raytheon ITSS, Greenbelt, Md., May 1997.

Wilkins, G. A., A new determination of the elements of the orbits of the satellites of Mars, in *Theory of Orbits in the Solar System and in Stellar Systems,* edited by G. Contopoulos, pp. 271-273, Academic, San Diego, Calif., 1967.

Yoder, C. F., and E. M. Standish, Martian precession and rotation from Viking lander range data, *J. Geophys. Res., 102*(E2), 4065-4080, 1997.

Yuan, D.-N., W. L. Sjogren, A. S. Konopliv, and A. B. Kucinskas, The gravity field of Mars: A 75th degree and order model, *J. Geophys. Res.,* this issue.

Zuber, M. T., D. E. Smith, S. C. Solomon, D. O. Muhleman, J. W. Head, J. B. Garvin, J. B. Abshire, and J. L. Bufton, The Mars Observer Laser Altimeter investigation, *J. Geophys. Res., 97,* 7781-7797, 1992.

Zuber, M. T., et al., Internal structure and early thermal evolution of Mars from Mars Global Surveyor topography and gravity, *Science, 287,* 1788-1793, 2000.

D. S. Chinn and D. E. Pavlis, Raytheon ITSS Corp.,4400 Forbes Boulevard, Lanham, MD 20706-4333, USA. (dchinn@geodesy.gsfc.nasa.gov; dpavlis@geodesy2.gsfc.nasa.gov)

F. G. Lemoine, D. D. Rowlands, and D. E. Smith, Laboratory for Terrestrial Physics, NASA Goddard Space Flight Center, Code 920, Greenbelt, MD 20771, USA. (flemoine@geodesy2.gsfc.nasa.gov; drowland@helmert.gsfc.nasa.gov; dsmith@tharsis.gsfc.nasa.gov)

G. A. Neumann and M. T. Zuber, Department of Earth, Atmospheric, and Planetary Sciences, Massachusetts Institute of Technology, 54-518, Cambridge, MA 02139-4307, USA. (neumann@tharsis.gsfc.nasa.gov; zuber@mit.edu)